Asparagine availability controls germinal centre B cell homeostasis

Eros Marin[1],
Karolina Bentkowska[1],
Yavuz Yazicioglu[1],
Alexander J. Clarke[1,*]

1. Kennedy Institute of Rheumatology, University of Oxford, Oxford, UK

* Corresponding author (alexander.clarke@kennedy.ox.ac.uk)

Abstract

Germinal centre (GC) B cells proliferate at some of the highest rates of any mammalian cell. Yet the metabolic processes which enable this are poorly understood. We performed integrated metabolomic and transcriptomic profiling of GC B cells, and found that metabolism of the non-essential amino acid asparagine is highly upregulated. Asparagine is conditionally essential to B cells, and its synthetic enzyme, asparagine synthetase (ASNS) is markedly upregulated following their activation, through the integrated stress response sensor general control non-derepressible 2 (GCN2). When *Asns* is deleted, B cell survival in low asparagine conditions is severely impaired, and removal of environmental asparagine by asparaginase severely compromises the GC reaction. Using stable isotope tracing, we found that metabolic adaptation to the absence of asparagine requires ASNS, and that the synthesis of nucleotides is particularly sensitive to asparagine deprivation. Conditional deletion of *Asns* in B cells selectively impairs GC formation, revealing that asparagine acts as a gate for RNA synthesis.

Introduction

The germinal centre (GC) reaction is essential for effective humoral immunity[1]. Following encounter with antigen, B cells organise in secondary lymphoid tissue and enter the GC reaction, a cyclic process in which somatic hypermutation (SHM) leads to random mutation of immunoglobulin genes. B cells then compete to interact with and receive help from T follicular helper cells. This process continues as affinity maturation occurs and memory B cells or plasma cells are generated.

GC B cells have some of the highest proliferation rates of all cells, yet their metabolism is unusual and incompletely understood[2]. Unlike most rapidly dividing immune cells, GC B cells predominantly use fatty acid oxidation and OxPhos rather than glycolysis[3–6], despite residing in a hypoxic and poorly vascularised micro-environment[7]. Which other specific metabolic pathways are important in their homeostasis has not been fully defined.

Amino acid availability is a critical regulator of T cell responses, demonstrated either by alteration of environmental abundance, synthesis, or interference with cellular import through solute transporters[8–12]. Amino acids are fundamentally required for protein synthesis, but are central to other metabolic processes[13], and it is apparent in T cells that availability of specific amino acids can have profound effects of their homeostasis.

In contrast, although it is known that B cell-derived lymphomas are sensitive to amino acid deprivation[14–17], and whilst loss of the capacity to synthesise serine, or deletion of CD98, a component of large neutral amino acid transporters, impairs GC formation, the importance of

amino acid availability more broadly in B cell metabolism and humoral immunity is poorly understood[18].

Here, we find that GC B cells have high levels of amino acid uptake and protein synthesis. Using integrated pathway analysis we identify asparagine (Asn), a non-essential amino acid, as a critical regulator of GC formation and B cell homeostasis. In vivo, mice with conditional deletion of asparagine synthetase (ASNS) in B cells have selective impairment of GC formation, and depletion of environmental Asn strongly suppresses the GC reaction. ASNS is regulated by sensing through the integrated stress response, and whilst most Asn in B cells is obtained from the extracellular environment following activation, mechanistically, loss of ASNS leads to profound metabolic dysfunction characterised by failure of nucleotide synthesis.

Results

GC B cells have highly active protein synthesis

To evaluate protein synthesis rates in GC B cells, we immunised mice with sheep red blood cells (SRBC) and first examined expression of CD98, which forms heterodimers with the amino acid transporter proteins SLC7A5 and SLC3A2 to form L-type amino acid transporter 1 (LAT1), at day 9 following immunisation. As previously reported, CD98 was markedly upregulated in GC B cells compared with IgD^+ naïve B cells (Fig. 1A-B)[18], suggesting high amino acid uptake. To more directly estimate protein synthesis rates in GC B cells in vivo and in their spatial context, we used bio-orthogonal non-canonical amino acid tagging, with the amino acid analogues O-propargyl-puromycin (OPP), and L-azidohomoalanine (L-AHA), visualised in situ using Click chemistry[19]. OPP is a puromycin analogue that enters the acceptor site of ribosomes, and is incorporated into nascent proteins. L-AHA is a methionine analogue, which does not lead to ribosomal stalling once included in polypeptides. To label GC B cells, we immunised mice expressing $Rosa26^{STOP}$tdTomato under the control of *Aicda*-Cre with SRBC. This labels cells which have expressed activation-induced cytidine deaminase (AID), the enzyme responsible for SHM and expressed following B cell activation, with the fluorescent protein tdTomato. At day 14, we first injected a pulse of L-AHA and then after four hours a pulse of OPP, sacrificing mice one hour later (Fig. 1C). We then used Click chemistry to label splenic sections. We found that incorporation of L-AHA and OPP were markedly upregulated in the GC compared with the surrounding follicle of naïve B cells, indicating highly active protein synthesis (Fig. 1D). We also labelled GC B cells with OPP ex vivo, and quantified its incorporation by flow cytometry (Fig. 1E). This confirmed a significant increase in OPP signal in GC B cells compared with follicular B cells. Within the GC B cell population, signal was highest in dark zone GC B cells, which are undergoing proliferation and SHM. GC B cells therefore have high rates of both amino acid transporter expression and protein synthesis.

Asparagine metabolism is upregulated in GC B cells

We next directly profiled the metabolite content of GC B cells. To do so, we isolated GC and naïve B cells from pools of wild type mice following immunisation with SRBC and quantified key metabolites using LC-MS (Fig. 2A). This revealed a broad increase in the levels of metabolites in GC B cells, with overrepresentation of intermediates of glycolysis, the TCA cycle, and most amino acids (Fig. 2B). Notably however, nucleotide precursor molecules were depleted in GC B cells, potentially reflective of their consumption during the nucleic acid synthesis required for high rates of proliferation. To refine our approach, we fused metabolite and transcriptional datasets[20] and performed integrated pathway analysis on the

combined data using hypergeometric set testing (Fig. 2C). We found that there was enrichment of amino acid metabolic pathways in GC B cells, most notably the Kyoto Encyclopedia of Genes and Genomes (KEGG) Alanine, Aspartate, and Glutamate (AAG) metabolism pathway. Examination of the leading-edge genes of the AAG pathway in an independent transcriptional dataset revealed an approximately 40-fold increase in the expression of asparagine synthetase (*Asns*) and a 15-fold increase in glutamic oxaloacetic transaminase-2 (*Got2*) in GC B cells compared with naïve B cells (Fig. 2D)[21]. ASNS synthesises Asn from aspartate (Asp) in an ATP-dependent reaction, and GOT2 synthesises Asp from the TCA cycle intermediate oxaloacetate (Fig. 2E)[22]. The levels of both Asn and Asp were markedly increased in GC compared with naïve B cells, which had equivalent glutamate levels (Fig. 2F), and we confirmed upregulation of *Asns* and *Got2* in sorted GC B cells by qPCR or western blotting (Fig. 2G-H). Asn metabolism is therefore one of the most upregulated pathways in GC B cells, suggesting that it may play a key role in their homeostasis.

Asns is selectively required by GC B cells

To determine if Asn synthesis is required for B cell development or GC formation, we conditionally deleted *Asns* under the control of *Cd79a*-Cre (B-Asns hereafter)(Extended Data Fig. 1A), which is active at the earliest stages of B cell development[23]. Whilst B cell development in the bone marrow and periphery was intact in B-Asns mice, following immunisation with SRBCs, splenic GC B cells were significantly reduced proportionately and numerically at day 9, and GCs were smaller (Fig. 3A-C). There was an increase in the ratio of GC B cells with dark zone to light zone markers (Fig. 3D). There were no differences in the proportions of splenic plasma cells (Fig. 3E). GC B cells from intestinal Peyer's patches, which form in response to microbiota, were also decreased in B-Asns mice (Fig. 3F).

We next examined the effect of *Asns* deletion in B cells on the generation of an antigen-specific immune response by immunising mice with 4-hydroxy-3-nitrophenylacetyl-chicken gamma globulin (NP-CGG) in alum. At day 14, the frequency of NP-binding GC B cells, and accordingly the usage of the Igλ light chain which dominates the anti-NP immune response[24], was significantly reduced in the B cell pool in B-Asns mice (Fig. 3G-H).

We then performed transcriptional profiling of B-Asns and B-WT GC B cells, following immunisation with SRBC (Fig. 3I). Using gene set enrichment analysis, we found upregulation of pathways associated with the endoplasmic reticulum (ER) stress response to misfolded proteins, and downregulation of B cell activation gene sets.

To determine whether the defect in GC B cell numbers was cell intrinsic, we generated mixed competitive bone marrow chimeras with wild type CD45.1 mice and either CD45.2 B-WT or B-Asns mice. There were no differences in reconstitution of the peripheral B or T cell compartment at week 11 (Extended Data Fig. 1E-F) in keeping with the dispensable role of *Asns* in B cell development . However, following immunisation with SRBC, CD45.2 B-Asns B cells represented a significantly lower proportion of the GC B cell pool compared with B-WT mice (Fig. 3J).

Finally, to understand the effect of systemic Asn deprivation on the GC reaction, we immunised Blimp1-mVenus reporter mice with SRBC, to be able to identify plasma cells, and administered L-asparaginase (ASNase), an *E. coli*-derived enzyme which hydrolyses Asn to aspartic acid and ammonia (Fig. 3L). ASNase had minimal effects on total $CD19^+$ B cells, plasma cells, or $CD3^+$ T cells, but profoundly reduced GC B cell numbers (Fig. 3M and

Extended Data Fig. 1G). Asn, both endogenously synthesised and from the environment, is therefore selectively essential for GC B cell homeostasis.

Asn controls B cell homeostasis

Asparagine is a non-essential amino acid and can be either acquired exogenously or synthesised by ASNS. To understand the dynamics of Asn uptake following B cell activation, we first stimulated wild type B cells *in vitro* with either the TLR9 agonist CpG and agonistic anti-CD40 antibody, or IL-4 and anti-CD40, for 24h in the presence of ^{15}N-labelled Asn, and quantified amino acids by mass spectrometry. We found a generalised increase in the intracellular concentrations of most amino acids, but in particular proline, glutamate, and asparagine (Fig. 4A). The majority of Asn was labelled with ^{15}N in all conditions, indicating high exogenous uptake, and in preference to endogenous synthesis, which is bioenergetically demanding (Fig. 4B).

Next, to determine the requirements of B cells for exogenous asparagine, we stimulated them with agonistic anti-CD40 and CpG or IL-4 in RPMI-1640 media with varying concentrations of Asn. Standard RPMI-1640 contains supraphysiologic concentrations of Asn (378μM) compared with those found in plasma (~40μM) and cerebrospinal fluid (~4μM)[25,26].

We found that Asn was conditionally essential for B cell viability and proliferation, determined by stimulus and the time point at which Asn was removed. When B cells were deprived of Asn or supplemented with 4μM Asn and stimulated with IL-4 and anti-CD40 for 72h, there was a severe reduction in cell viability and proliferation, compared with supplementation of Asn at plasma or supraphysiological concentrations (Fig. 4C-D). Importantly, we noted no decrease in cell proliferation or viability on withdrawal of exogenous aspartate or glutamate, although glutamine was required for B cell survival as previously described[27] (Fig. 4E and Extended Data Fig. 2A). There was a reduction in the expression of the activation markers CD86 and MHCII following Asn deprivation, nascent protein synthesis measured by OPP incorporation was reduced at 24h (Extended Data Fig. 2B-D), and apoptosis was increased (Extended Data Fig. 2E).

However, when B cells were stimulated with IL-4 and anti-CD40 with Asn for 72h and then subsequently deprived of Asn for a further 24h, there were minimal differences in survival, but proliferation and OPP incorporation were slightly reduced (Fig. 4F and Extended Data Fig. 2F). This indicated that Asn was essential for survival and cell division in the early stages of B cell activation, but became less important later. Minimal differences in viability or proliferation with Asn deprivation were also seen when B cells were stimulated with CpG and anti-CD40 (Fig. 4G). The capacity of B cells to survive without Asn was therefore both time and stimulus dependent.

To understand if this may be mediated by acquisition of the capacity to synthesise Asn, we next examined the kinetics of ASNS expression. Transcription of *Asns* and expression of ASNS protein steadily increased following stimulation with IL-4 and CD40 (Fig. 4H-I). When Asn was excluded from media, *Asns* transcription and protein abundance were temporarily increased, but then fell below levels seen with Asn supplementation after 48h. We found there was synergistic upregulation of ASNS when B cells were stimulated with both IL-4 and anti-CD40 (Fig. 4J).

Survival and proliferation of B-Asns B cells were severely compromised in the absence of Asn, but were normal when Asn was present (Fig. 4K). When B-Asns B cells were pre-

stimulated in the presence of Asn, which was then withdrawn, the previously demonstrated protective effect of activation was attenuated, and their ability to synthesise IgM and IgG1 was diminished (Extended Data Fig 2G), although their viability was still much higher than if Asn was never present (Fig. 4L).

Asns is known to be upregulated following activation of the integrated stress response (ISR), which occurs as a consequence of a variety of cellular stressors, including amino acid withdrawal[28,29]. A key event in the ISR is the phosphorylation of elongation initiation factor 2 alpha (eIF2α) by the kinase general control non-repressible-2 (GCN2). Phosphorylated eIF2α then controls transcription and translation of the ISR effector molecule activating transcription factor-4 (ATF4).

We examined *Gcn2*$^{-/-}$ B cells, and found that their survival was reduced following asparagine withdrawal, although paradoxically to a lesser extent that those from wild type mice (Fig. 4M). However, their proliferation was severely impaired. Upregulation of ASNS was substantially decreased in *Gcn2*$^{-/-}$ B cells, as was ATF4, which was otherwise robustly upregulated in the absence of Asn (Fig. 4N-O and Extended Data Fig. 2H). We did not detect an increase in expression of *Zbtb1*, which has been recently reported to regulate *Asns* expression (Extended Data Fig. 2I)[30].

Asn uptake is therefore particularly and specifically important during initial B cell activation, before the GCN2-dependent expression of ASNS, and acts to support cellular homeostasis.

ASNS gates nucleotide synthesis in B cells

An important characteristic of Asn is that it has functions outside of proteinogenesis, and in particular has been shown to regulate mTORC1 signalling, and maintain nucleotide synthesis when the electron transport chain is inhibited[31,32]. However, it remains unclear to what extent this may affect normal, non-malignant cells. We observed a significant reduction in mTORC1 activation assessed by phosphorylation of 4E-BP1 when B cells were stimulated without Asn, which was more pronounced in those from B-Asns mice (Fig. 4O). We also observed a reduction in mitochondrial mass and reactive oxygen species generation following Asn deprivation (Extended Data Fig. 3A-B).

To understand how Asn withdrawal affects B cell metabolism, we performed stable isotope resolved LC-MS on B cells from B-WT or B-Asns mice, stimulated for 72h in Asn-replete media, before switching for 24h into media with or without Asn, and [U-^{13}C]-glutamine, or $^{15}N_1$-glutamine, labelled at either the amine or amide nitrogen position. Since ASNS transfers the amide nitrogen group of glutamine to that of asparagine (acting as an amidotransferase), positional labelling can provide information on ASNS activity[22].

Intracellular Asn levels were greatly reduced in Asn-deprived conditions in both B-WT and B-Asns B cells, confirming our previous observation that exogenous uptake is dominant, but to significantly greater degree in those from B-Asns mice (Fig. 5A-B). B-WT cells did not engage in significant Asn synthesis when Asn was present, with negligible labelling of Asn with Gln-derived ^{15}N from either the amino or amide position (Fig 5C). Following Asn deprivation, around half of the intracellular Asn pool was ^{15}N-labelled in B-WT B cells, reflecting de novo synthesis by ASNS. As expected B-Asns B cells were incapable of Asn synthesis and no Asn was ^{15}N labelled. There was minimal labelling of Asn from ^{13}C glutamine, but around a quarter of Asp was labelled, with no difference between B-WT and B-Asns B cells, suggesting very little of the Gln-derived Asp pool was diverted to Asn synthesis (Fig. 5D, Extended Data Fig. 3C).

In B-WT cells, Asn deprivation had subtle effects on metabolite relative abundance, but significantly reduced fractional labelling from [U-^{13}C]-glutamine and $^{15}N_1$-glutamine. Despite small differences in intracellular Asn, B-Asns B cells exhibited profound metabolic dysfunction upon Asn withdrawal, with large reductions in metabolite relative amounts and glutamine-derived ^{15}N incorporation (Fig. 5E).

We next performed pathway analysis to systemically describe these results. Comparing B-WT and B-Asns B cells, both deprived of Asn, there were a common set of significantly different pathways (Fig. 5F), including AAG, tRNA biosynthesis, glutathione synthesis, sphingolipid metabolism and glyoxylate metabolism. B-Asns B cells deprived of Asn downregulated metabolites in nucleotide synthesis pathways, shown in detail in Fig. 5G. We correlated this with transcription of genes encoding enzymes within this pathway, and found that like metabolite abundance, there were minimal differences in gene expression between B-Asns and B-WT B cells in the presence of asparagine, but substantial differential expression when asparagine was absent (Fig. 5H).

Finally, to confirm defective nucleotide synthesis in ex vivo GC B cells, we examined RNA synthesis rates by measuring incorporation of the modified nucleotide 5-ethinyl uridine (5-EU) into nascent RNA of B-WT and B-Asns mice. We found that as expected given our measurements of protein synthesis, 5-EU incorporation was much higher in GC B cells than IgD$^+$ naïve B cells. However, in B-Asns GC B cells, this was significantly reduced, a difference not observed in naïve B cells (Fig. 5I).

Asn is therefore essential to regulate B cell metabolic homeostasis, and if it cannot be obtained in sufficient amounts from the environment or synthesised by ASNS, there is impairment of TCA cycle metabolism, and failure of nucleotide and RNA synthesis.

Discussion

Here we show that Asn metabolism is upregulated in GC B cells, and that deprivation of Asn either from the external environment or by inhibition of its synthesis strongly alters cellular metabolism, and in particular downregulates nucleotide and consequently RNA synthesis.

We found that GC B cells had high levels of protein synthesis *in vivo*, and highly expressed the amino acid transporter protein CD98. This corresponded with a preference for uptake of extracellular Asn, which was greatly increased following activation. Initial stimulation with Asn provided a protective effect against subsequent Asn withdrawal, as also observed in CD8$^+$ T cells[11,33], which we found was mediated in part by upregulation of ASNS, which was almost undetectable in naïve B cells. The residual survival benefit observed in pre-stimulated B-Asns cells may be mediated by cellular reserves of Asn, or by a lower requirement for Asn once activation has occurred, and this is supported by our finding that deprivation of Asn substantially impairs B cell activation. An interesting observation was the unexpected resilience of plasmablasts to either *Asns* deletion or ASNase. It is possible that their high expression of amino acid transporters, reliance on autophagy, or upregulation of the unfolded protein response are protective mechanisms in the face of Asn shortages[34,35].

A key finding was that Asn availability acts to gate nucleotide synthesis. GC B cells have high rates of RNA synthesis, in keeping with their active translational programming, and our LC-MS data revealed low levels of nucleotides, suggestive of their consumption. Analysis of Asn synthesis from glutamine showed that even following activation, which was associated with upregulation of ASNS, the great majority of Asn was exogenously acquired.

Nonetheless ASNS was essential for metabolic homeostasis and nucleotide synthesis, despite seemingly modest rates of Asn synthesis. This raises the interesting question of whether ASNS might have other, non-synthetic functions, as has been recently demonstrated for the enzyme phosphoglycerate dehydrogenase (PHGDH), whose canonical function is to synthesise serine[36]. The relationship between amino acid availability and nucleotide synthesis has been previously defined through mTORC1 signalling, acting via phosphorylation of carbamoyl-phosphate synthetase 2, aspartate transcarbamoylase, dihydroorotase (CAD), or the tetrahydrofolate cycle[37,38]. It is possible that in GC B cells, Asn availability tunes these nucleoside synthetic pathways, either through mTOR or other mechanisms.

ASNase has been a cornerstone of the treatment of leukaemia for decades, but ASNS may also be a novel therapeutic target in non-malignant, autoimmune disease, and is deserving of future study in this context.

Figure and legends

Figure 1

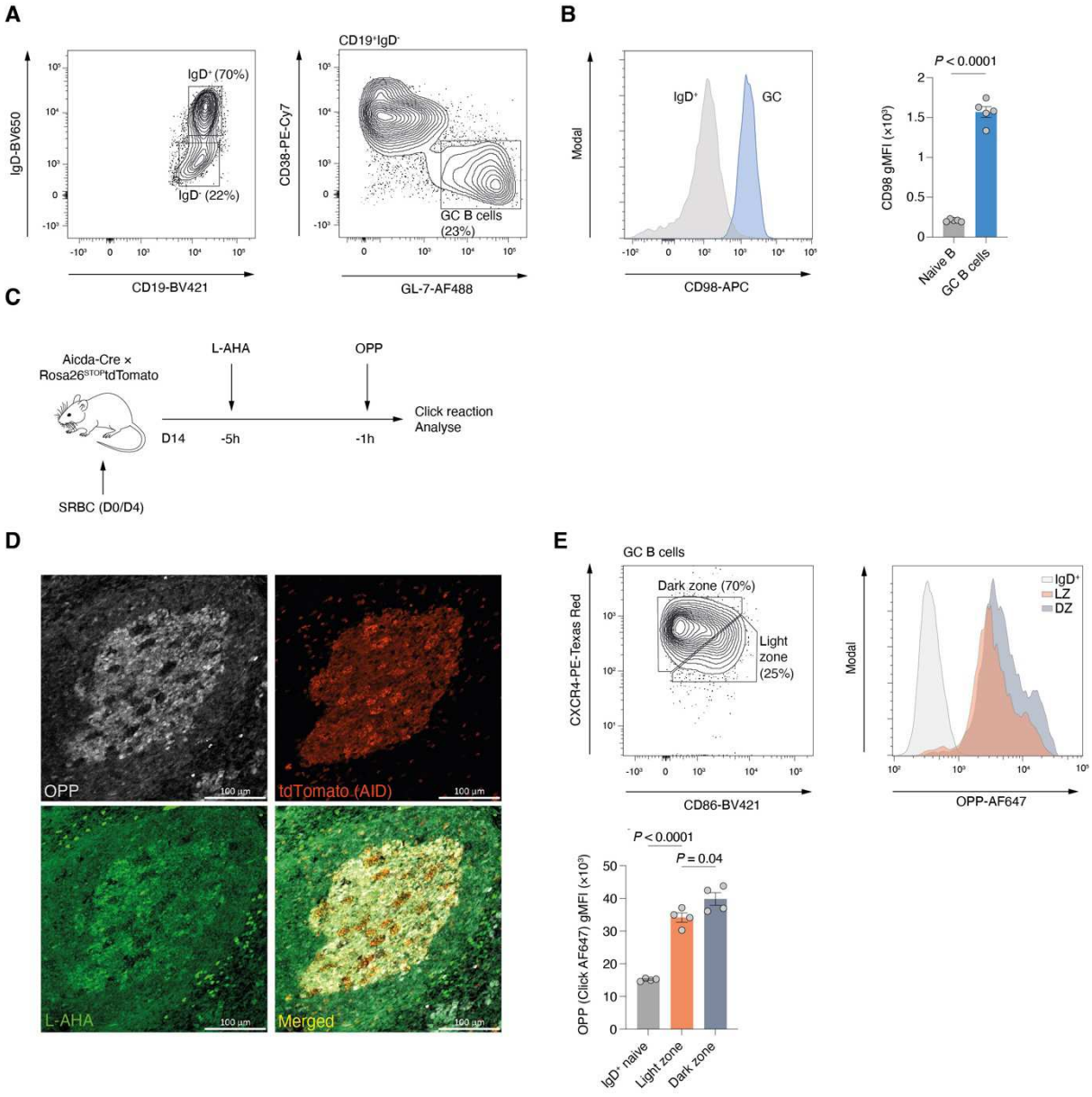

Figure 1. GC B cells have highly active protein synthesis

- **A.** Gating strategy for GC B cells ($CD19^+IgD^{lo}CD38^-GL\text{-}7^+$) and naïve IgD^+ B cells ($CD19^+IgD^+$).
- **B.** Representative flow cytometry histogram and quantification of CD98 geometric mean fluorescence intensity (gMFI) in IgD^+ naïve and GC B cells (n=5 mice). Data representative of two independent experiments.
- **C.** Schematic of in vivo bio-orthogonal non-canonical amino acid tagging. Aicda-cre × $Rosa26^{STOP}$tdTomato mice were immunised with SRBC and then boosted at day 4. At day 14, they were injected with L-AHA, and then four hours later with OPP. They were sacrificed one hour later, and non-canonical amino acid incorporation into splenic tissue was revealed using Click chemistry.

D. Representative immunofluorescence images of splenic GCs labelled with OPP, tdTomato (AID), and L-AHA. Representative of two independent experiments. Scale bar: 100μm.

E. Gating strategy, histogram, and quantification of OPP incorporation for light ($CD86^{hi}CXCR4^{lo}$) and dark zone ($CD86^{lo}CXCR4^{hi}$) GC B cells (n=4 mice). Representative of two independent experiments.

Statistical significance was determined by unpaired two-tailed t test (B) or one-way ANOVA with Tukey's multiple testing correction (E). Data are presented as the mean +/- SEM.

Figure 2

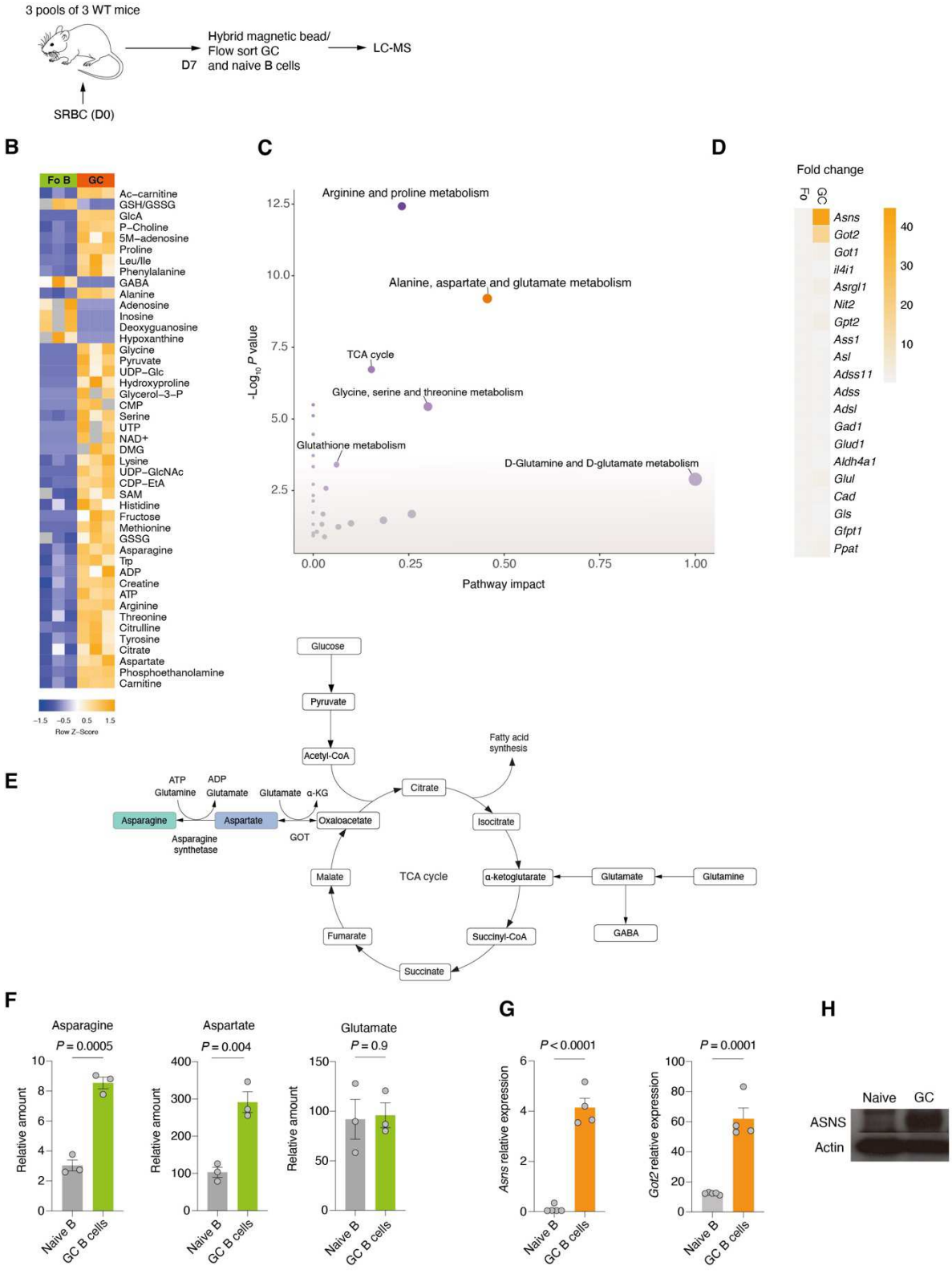

Figure 2. Asparagine metabolism is upregulated in GC B cells

- **A.** Schematic of experimental design. Three pools of three WT mice were immunised with SRBC, and at day 7 GC and follicular B cells were isolated by a hybrid magnetic bead and flow sorting approach, before analysis of polar metabolites by LC-MS.
- **B.** Heatmap of significantly differentially abundant metabolites (P_{adj} <0.05) in naïve and GC B cells at day 7 from wild type mice immunised with SRBC, measured by LC-mass spectrometry (n=3 pools of 3 mice/pool). Representative of two independent experiments.
- **C.** Integrated pathway analysis of differentially abundant metabolites from **A** and expressed genes from Immgen in GC compared to naïve B cells.
- **D.** Heatmap of relative gene expression of KEGG Alanine, Aspartate, and Glutamate pathway in GC vs naïve B cells, represented as fold change. Data are from GSE133971[21].
- **E.** Diagram of asparagine synthesis and its association with the TCA cycle.
- **F.** Relative amounts of asparagine, aspartate, and glutamate in GC and naïve B cells measured by LC-mass spectrometry (n=3 pools of 3 mice) as in **A**. Representative of two independent experiments.
- **G.** Relative expression of *Asns* and *Got2* in flow-sorted GC and naïve B cells from wild type mice immunised with SRBC at day 7, normalised to *Ubc* (n=4 mice). Representative of two independent experiments.
- **H.** Western blot of ASNS in GC and naïve B cells, purified by magnetic beads, at day 12 following enhanced immunisation with SRBC. Representative of two independent experiments.

Statistical significance was determined by two-way ANOVA with Tukey's multiple testing correction (A), hypergeometric test (B), or unpaired two-tailed t test (F-G). Data are presented as the mean +/- SEM.

Figure 3

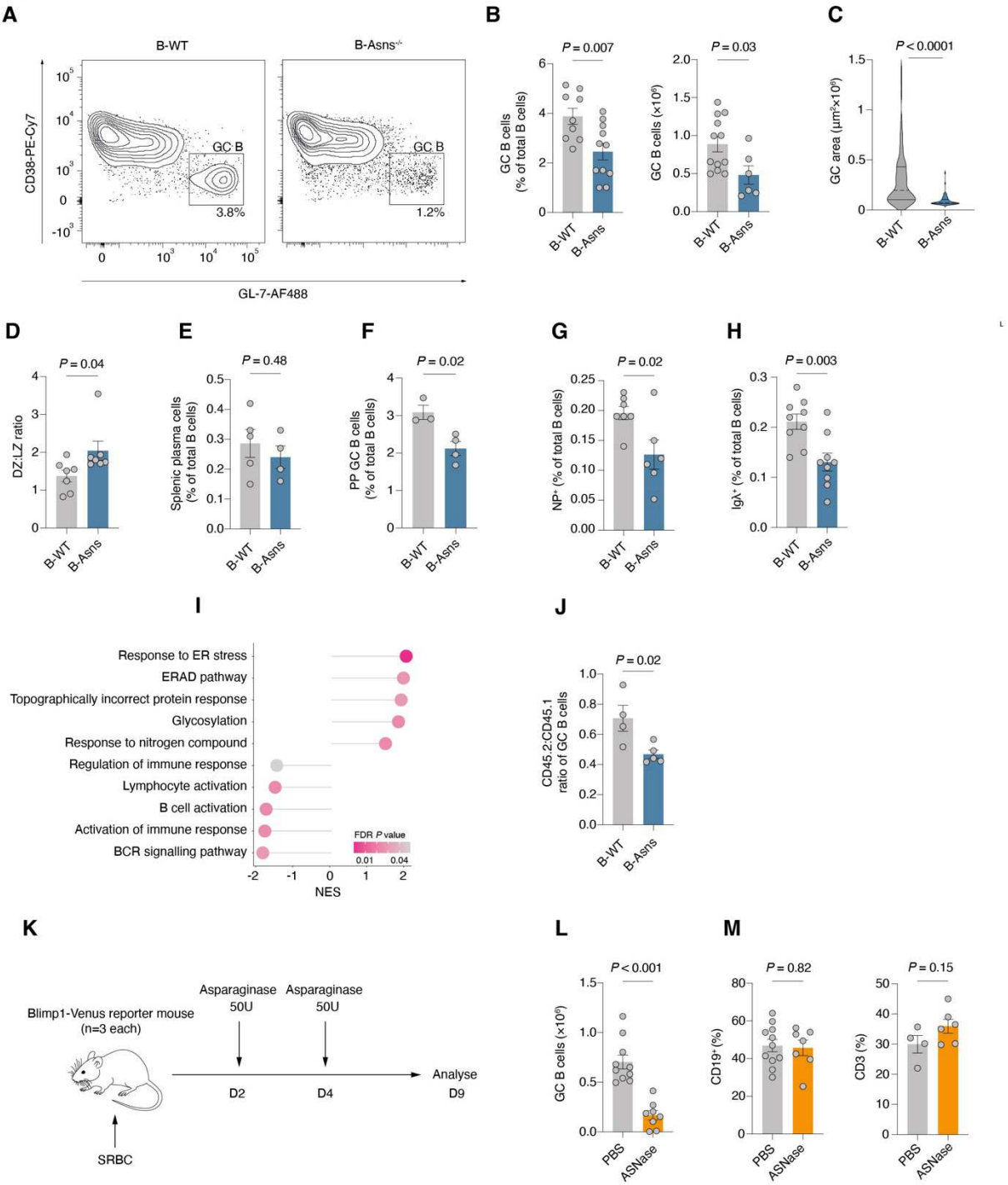

Figure 3. *Asns* is selectively required by GC B cells

- **A.** Representative flow cytometry plot of GC B cells ($CD19^+IgD^{lo}CD38^-GL\text{-}7^+$) at day 9 post-immunisation with SRBC, from B-WT and B-Asns mice.
- **B.** Quantification of proportion and number of GC B cells at day 9 following SRBC immunisation (n=9 B-WT and n=11 B-Asns). Data pooled from four independent experiments.
- **C.** Quantification of splenic GC surface area in μm^2 in B-WT and B-Asns mice. Each point represents a GC. Representative of 3 biological replicates per genotype.

D. Ratio of DZ:LZ ($CXCR4^{hi}CD86^{lo}$:$CXCR4^{lo}CD86^{hi}$) GC B cell populations (n=7 B-WT and n=7 B-Asns mice). Data pooled from two independent experiments.
E. Proportion of $CD138^{+}$ plasma cells in spleens of mice immunised with SRBC at day 9 (n=5 B-WT and n=4 B-Asns). Data pooled from two independent experiments.
F. Proportion of GC B cells in Peyer's patches (n=3 B-WT and n=4 B-Asns mice).
G. Proportion of NP-binding splenic GC B cells at day 14 following immunisation with NP-CGG (n=7 B-WT and n=6 B-Asns mice). Data pooled from three independent experiments.
H. Proportion of $Ig\lambda^{+}$ GC B cells at day 14 following immunisation with NP-CGG (n=9 B-WT and n=9 B-Asns). Data pooled from three independent experiments.
I. Gene set enrichment analysis plot of GO terms from RNA sequencing of GC B cells (n=3 B-WT and n=4 B-Asns mice) at day 9 following immunisation with SRBC.
J. Ratio of splenic CD45.2:CD45.1 GC B cells from competitive bone marrow chimeric mice (n=4 B-WT and n=5 B-Asns mice).
K. Schematic for asparaginase administration. Mice were immunised with SRBC and then 50IU of asparaginase or vehicle was administered by i.p. injection at day 2 and 4, with analysis at day 9.
L. Numbers of GC B cells at day 9 in Blimp1-Venus reporter mice following treatment with asparaginase at days 2 and 4 following SRBC immunisation (n=10 in control and n=8 in ASNase treatment groups). Representative of two independent experiments.
M. Effect of asparaginase on peripheral $CD3^{+}$ and $CD19^{+}$ populations as in **L**. Representative of two independent experiments.

Statistical significance was determined by unpaired two-tailed t test. Data are presented as the mean +/- SEM.

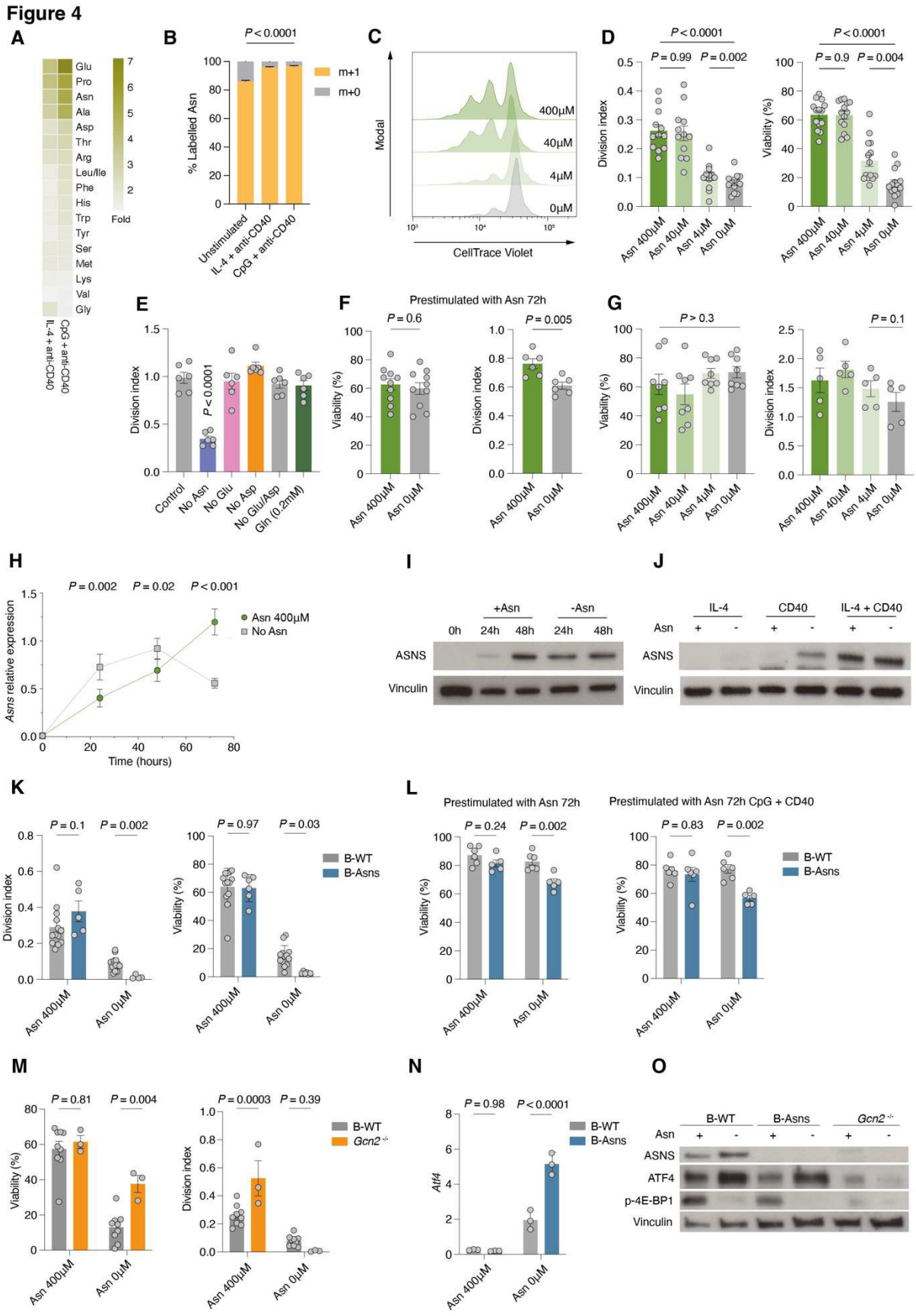

Figure 4. Asn controls B cell homeostasis

- **A.** Heatmap of fold change of indicated amino acids in B cells, measured by LC-mass spectrometry following stimulation for 24h with IL-4 and anti-CD40, or CpG and anti-CD40, relative to unstimulated condition (n=3 mice). Representative of two independent experiments.
- **B.** Fraction of labelling of intracellular Asn with ^{15}N in B cells stimulated as in **A**, in the presence of $^{15}N_1$-Asn (n=3 mice). Representative of two independent experiments.
- **C.** Representative histogram of dilution of Celltrace Violet in B cells stimulated with IL-4 and anti-CD40 and cultured for 72h with the indicated concentration of Asn.
- **D.** Viability and division index of B cells stimulated with IL-4 and anti-CD40 and cultured for 72h with the indicated concentration of Asn (n=10 mice). Representative of and pooled from three independent experiments.
- **E.** Division index of B cells stimulated for 72h with IL-4 and anti-CD40 in the presence or absence of the indicated amino acids (n=6 mice). Representative of and pooled from three independent experiments.
- **F.** Viability and division index of B cells stimulated with IL-4 and anti-CD40 with 400μM Asn for 72h, then restimulated for an additional 24h in the absence of Asn (n=10 mice). Representative of and pooled from two independent experiments.
- **G.** Viability and division index of B cells stimulated with CpG and anti-CD40 and cultured for 72h with the indicated concentration of Asn (n=8 mice). Representative of and pooled from three independent experiments.
- **H.** Quantification of relative expression of *Asns* at the indicated timepoints in B cells stimulated with IL-4 and anti-CD40 in the presence or absence of Asn (n=3 mice). Representative of two independent experiments.
- **I.** Representative immunoblot of ASNS in B cells stimulated for with IL-4 and anti-CD40 with or without Asn, at the indicated timepoints. Representative of two independent experiments.
- **J.** Representative immunoblot of ASNS in B cells stimulated for 48h with IL-4, anti-CD40, or IL-4 and anti-CD40, with or without Asn. Representative of two independent experiments.
- **K.** Viability and division index of B cells from B-Asns and B-WT mice stimulated for 72h with IL-4 and anti-CD40 in the presence or absence of Asn (n=13 B-WT and n=5-6 B-Asns mice). Representative of and pooled from >4 independent experiments.
- **L.** Viability and division index of B cells from B-Asns and B-WT mice stimulated with IL-4 and anti-CD40 or CpG and anti-CD40, with Asn for 72h, then restimulated for an additional 24h in the absence of Asn (n=6 B-WT and n=5-6 B-Asns mice). Representative of and pooled from two independent experiments.
- **M.** Viability of B-WT and *Gcn2*$^{-/-}$ B cells stimulated for 72h with IL-4 and anti-CD40, in the presence or absence of Asn (n=9 B-WT and n=3 *Gcn2*$^{-/-}$ mice). Representative of three independent experiments.
- **N.** Relative expression of *Atf4* in B-Asns and B-WT B cells stimulated for 72h in the presence or absence of Asn (n=3 B-WT and n=3 B-Asns mice). Representative of 2 independent experiments.
- **O.** Representative immunoblot for ASNS, ATF4, and phospho-4E-BP1 in B cells from B-Asns, *Gcn2*$^{-/-}$ and B-WT mice, stimulated for 24h with anti-CD40 and IL-4 in the presence or absence of Asn. Representative of two independent experiments.

Statistical significance was determined by one-way ANOVA with Tukey's multiple testing correction (B,D-E, G), unpaired two-tailed t test (F), or two-way ANOVA with Šidák's multiple testing correction (H, K-N). Data are presented as the mean +/- SEM.

Figure 5

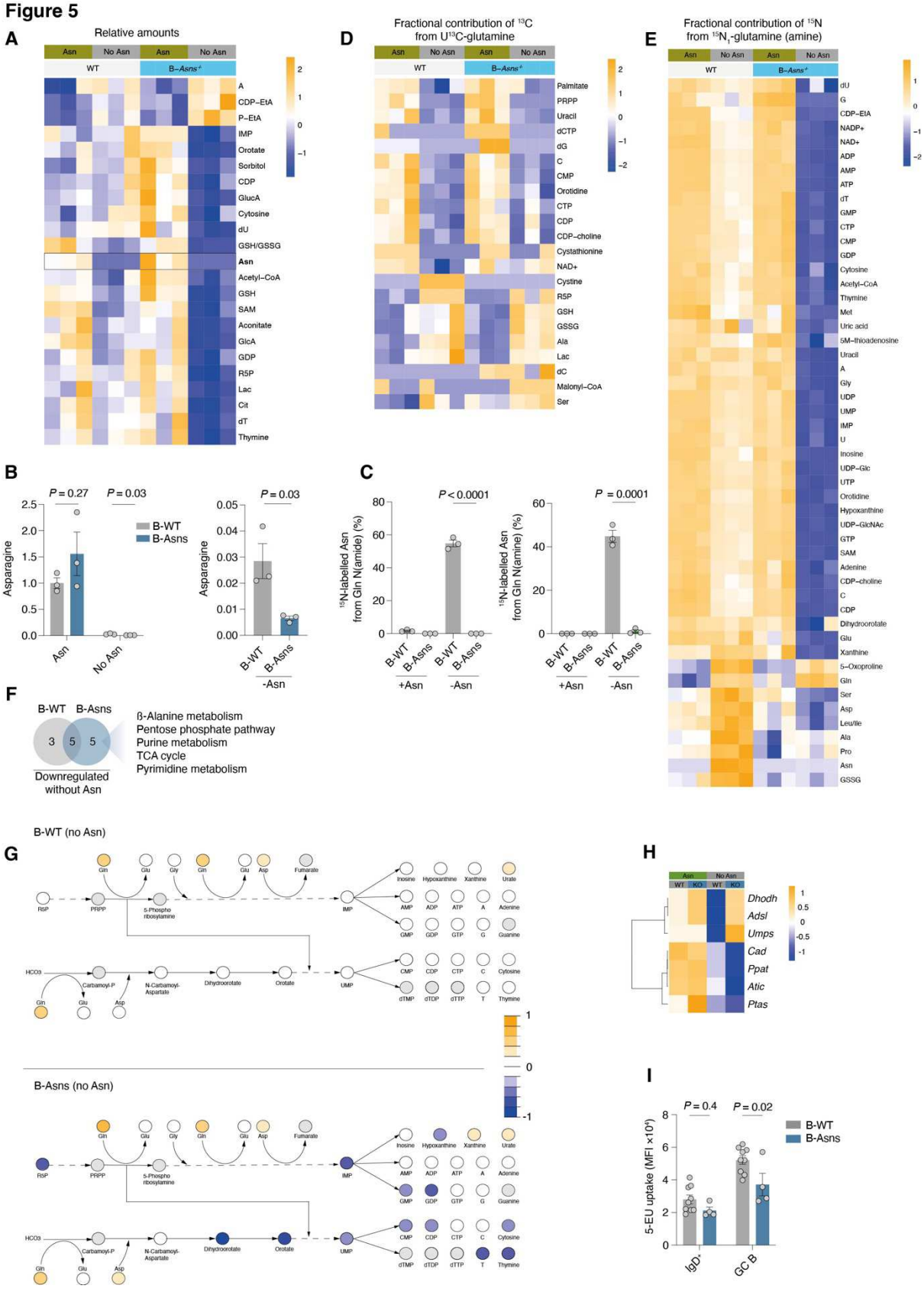

Figure 5. ASNS gates nucleotide synthesis in B cells

- **A.** Heatmap of relative amounts of significantly different metabolites in B cells from B-WT or B-Asns mice stimulated with IL-4 and anti-CD40 for 72h in the presence of 400μM Asn, then cultured for an additional 24h with or without 400μM Asn (n=3 B-WT and n=3 B-Asns mice). Scale represents row Z-score. Significantly differentially abundant metabolites ($P_{adj} < 0.05$) are shown. Representative of two independent experiments.
- **B.** Abundance of intracellular Asn in B cells cultured as in **A**, and rescaled plot of Asn-deprived condition. Representative of two independent experiments.
- **C.** Fractional contribution of ^{15}N to Asn pool, derived from $^{15}N_1$-amino or amide Gln, following culture as described in **A**, with labelled compound added for final 24h of culture.
- **D.** Heatmap of fractional contribution of ^{13}C to indicated metabolites, derived from U-^{13}C-Gln following culture as described in **A**, with labelled compound added for final 24h of culture. Scale represents row Z-score. Significantly differentially labelled metabolites ($P_{adj} < 0.05$) are shown.
- **E.** Heatmap of fractional contribution of ^{15}N to indicated metabolites, derived from $^{15}N_1$-amine Gln following culture as described in **A**, with labelled compound added for final 24h of culture. Scale represents row Z-score. Significantly differentially labelled metabolites ($P_{adj} < 0.05$) are shown.
- **F.** Venn-diagram indicating number of significantly differentially-regulated pathways in B-WT and B-Asns B cells following Asn-withdrawal, based on relative metabolite abundance as in **A**. Listed pathways are those specifically downregulated in B-Asns B cells.
- **G.** Relative abundance of metabolites in nucleotide synthesis pathway in B-WT and B-Asns B cells deprived of Asn, as in **A**. Grey-filled circles indicate that the metabolite was not detected. Scale represents abundance ratio.
- **H.** Heatmap of relative expression of indicated genes in B cells from B-Asns and B-WT mice cultured for 72h with IL-4 and anti-CD40 and quantified by RT-qPCR. Each heatmap cell represents the mean of 3 individual mice (B-WT and B-Asns). Representative of two independent experiments.
- **I.** 5-EU uptake for GC and IgD^+ naïve B cells (n=10 B-WT and n=4 B-Asns mice). Data pooled from three independent experiments.

Statistical significance was determined by two-way ANOVA with Šidák's multiple testing correction (A, B, C-E), hypergeometric test (F) or unpaired two-tailed t test (B, I). Data are presented as the mean +/- SEM.

Extended Data Figure 1

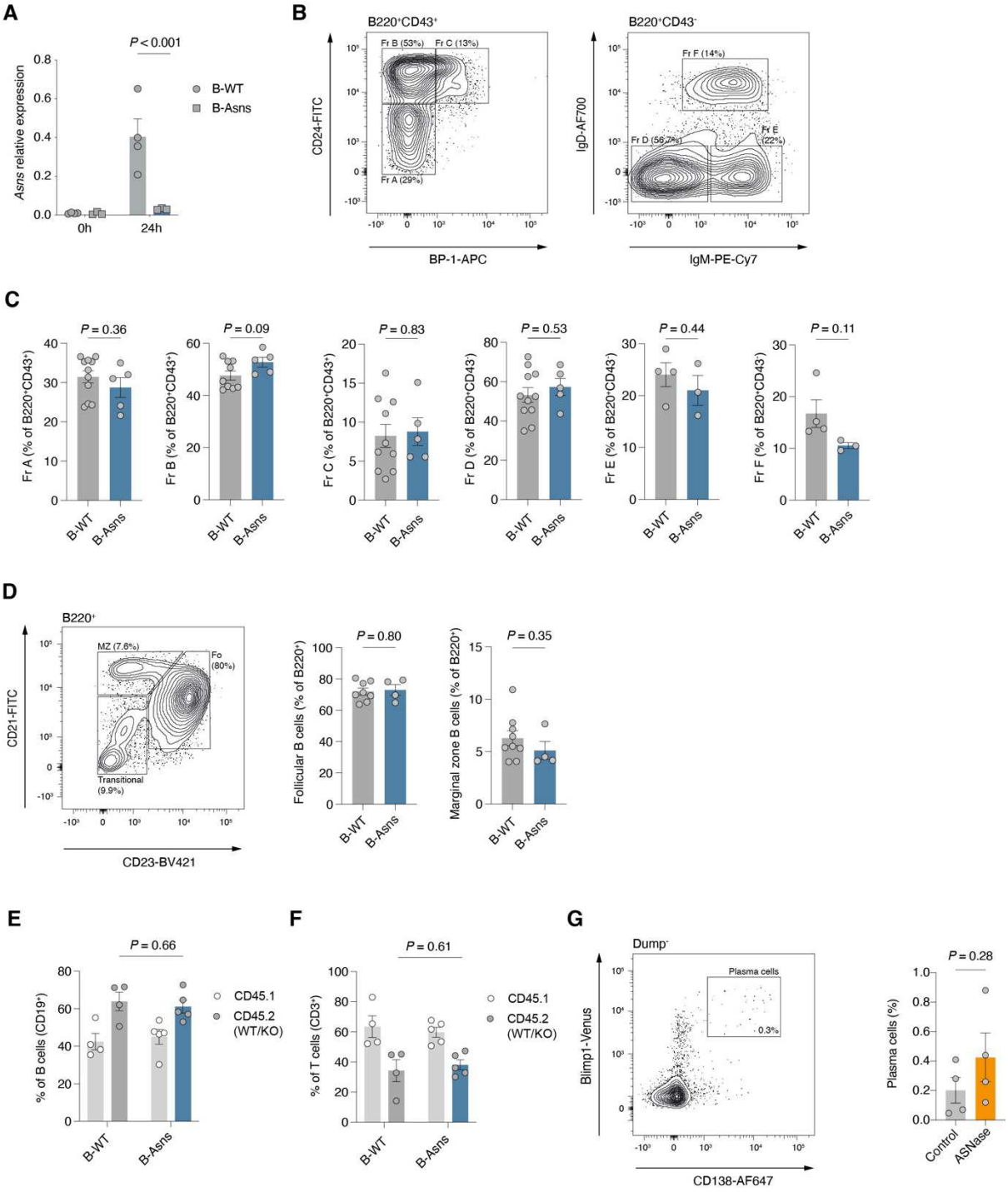

Extended Data Figure 1 – Deletion of *Asns* does not affect B cell development

A. Relative expression of *Asns* by qPCR in freshly isolated, and stimulated (IL-4 and anti-CD40 for 24h) B cells (n=4 B-WT and n=4 B-Asns mice). Representative of two independent experiments.

B. Representative gating strategy for indicated Hardy stages of B cell development in bone marrow.

C. Quantification of indicated Hardy stages of B cell development in bone marrow (n=11 B-WT and n=5 B-Asns mice). Data pooled from two independent experiments.

D. Representative gating strategy for transitional, marginal zone, and follicular B cells in spleen and quantification (n=8 B-WT and n=4 B-Asns). Data pooled from two independent experiments.

E. Reconstitution of total peripheral CD19^{+} B cell compartment in 50:50 competitive bone marrow chimera (as in Fig. **3J**).

F. Reconstitution of total peripheral CD3^{+} T cell compartment in 50:50 competitive bone marrow chimera (as in Fig. **3J**).

G. Representative flow cytometry gating strategy and quantification of plasma cells (Dump^{-}CD138^{hi}Blimp1-mVenus^{hi}) following asparaginase treatment. Representative of two independent experiments.

Statistical significance was determined by two-way ANOVA with Šidák's multiple testing correction (A, E-F) or unpaired two-tailed t test (C-D, G). Data are presented as the mean +/- SEM.

Extended Data Figure 2

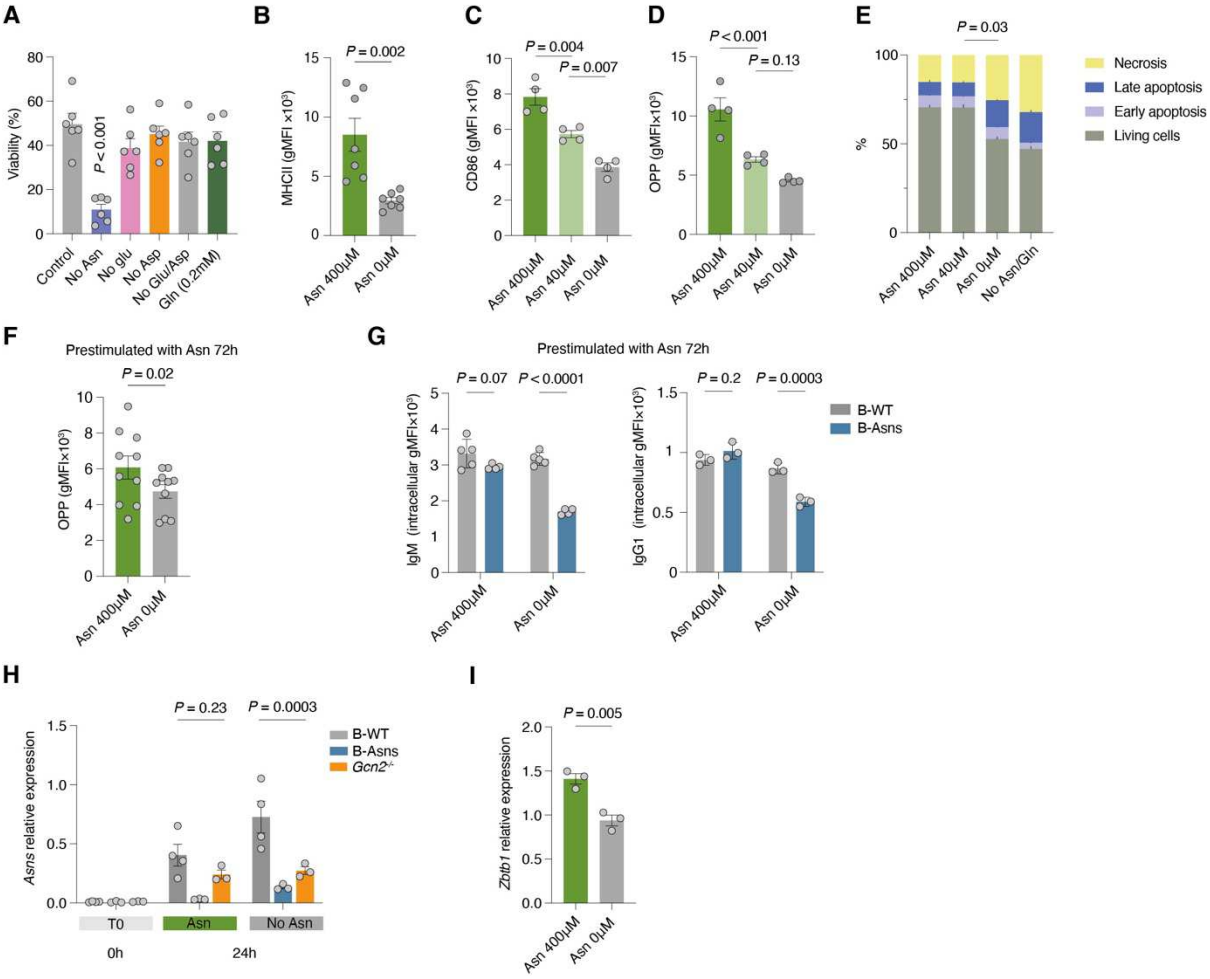

Extended Data Figure 2 – Asn regulates B cell homeostasis

- **A.** Viability of B cells stimulated for 72h with IL-4 and anti-CD40, in the presence or absence of the indicated amino acids (n=6 mice). Representative of three independent experiments.
- **B.** MHCII gMFI in B cells stimulated for 24h with IL-4 and anti-CD40 with the indicated concentrations of Asn (n=7 mice). Representative of and pooled from three independent experiments.
- **C.** CD86 gMFI in B cells stimulated for 24h with IL-4 and anti-CD40 with the indicated concentrations of Asn (n=4). Representative of three independent experiments.
- **D.** OPP incorporation determined by flow cytometry in B cells stimulated for 24h with IL-4 and anti-CD40 with the indicated concentrations of Asn (n=4). Representative of two independent experiments.
- **E.** Quantification of stages of apoptosis in B cells stimulated with IL-4 and anti-CD40 at 18h, defined by annexin V binding and propidium iodide staining, in the presence/absence of Asn or Asn and Gln (n=3 individual mice). Representative of two independent experiments.
- **F.** OPP uptake of B cells stimulated for 72h with IL-4 and anti-CD40 in the presence or absence of the indicated concentration of Asn (n=10). Representative of and pooled from two independent experiments.
- **G.** Quantification of intracellular IgM and IgG1 by flow cytometry in B cells stimulated with IL-4 and anti-CD40 with 400μM Asn for 72h, then restimulated for an additional 24h in the absence of Asn (n=5 B-WT and n=3-4 B-Asns mice). Representative of two independent experiments.
- **H.** Relative expression of *Asns* by qPCR in freshly isolated (T=0) and stimulated (IL-4 and anti-CD40 for 24h) B cells (n=4 B-WT, n=3 B-Asns, and n=3 *Gcn2*$^{-/-}$ mice). Representative of two independent experiments.
- **I.** Relative expression of *Zbtb1* by qPCR in B cells stimulated with IL-4 and anti-CD40 from wild type mice (n=3), in the presence or absence of Asn. Representative of two independent experiments.

Statistical significance was determined by one-way ANOVA with Tukey's multiple testing correction (A, E), unpaired two-tailed t test (B, F, I), or two-way ANOVA with Šidák's multiple testing correction (G-H). Data are presented as the mean +/- SEM.

Extended Data Figure 3

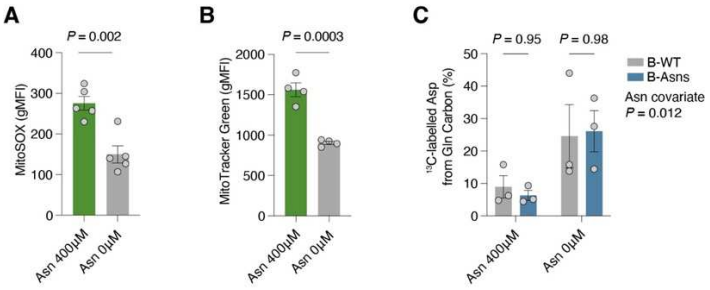

Extended Data Figure 3 – Asn controls mitochondrial mass

- **A.** MitoSOX gMFI of B cells stimulated with IL-4 and anti-CD40 from wild type mice, in the presence or absence of Asn (n=5 mice). Representative of two independent experiments.
- **B.** MitoTracker Green gMFI of B cells stimulated with IL-4 and anti-CD40 from wild type mice, in the presence or absence of Asn (n=4 mice). Representative of two independent experiments.
- **C.** Percentage of aspartate labelled with ^{13}C, indicating derivation from U^{13}C-glutamine, as in Fig. **5D**.

Statistical significance was determined by unpaired two-tailed t test (A,B), or two-way ANOVA with Šidák's multiple testing correction, with Asn concentration as a covariate (C). Data are presented as the mean +/- SEM.

Material and methods

Mice

C57BL/6J mice were obtained from Envigo. C57BL/6N-*Asns*$^{tm1c(EUCOMM)Wtsi}$/H (EM:05307) mice were obtained from the Mary Lyon Centre, MRC Harwell, UK. B6.129S6-*Eif2ak4*$^{tm1.2Dron}$/J (JAX: 008240) and B6.C(Cg)-*Cd79a*$^{tm1(cre)Reth}$/EhobJ (JAX: 020505) mice were obtained from Jackson Laboratories. Tg(Prdm1-Venus)1^{Sait} [Blimp1-mVenus] (MGI:3805969) mice were a kind gift from Mitinori Saitou (Kyoto University). B6.SJL.CD45.1 mice were provided by the central breeding facility of the University of Oxford. Male and female mice between the ages of 6-15 weeks were used. Mice were bred and maintained under specific pathogen-free conditions at the Kennedy Institute of Rheumatology, University of Oxford. They were housed in cages that had individual ventilation and were provided with environmental enrichment. The temperature was kept between 20-24°C, with a humidity level of 45-65%. They were exposed to a 12-hour cycle of light and darkness (7 am to 7 pm), with a thirty-minute period of dawn and dusk. All procedures and experiments were performed in accordance with the UK Scientific Procedures Act (1986) under a project license authorized by the UK Home Office (PPL number: PP1971784).

Bone marrow chimera generation

B6.SJL.CD45.1 recipient mice were administered two doses of 5.5Gy irradiation four hours apart. Mice were then intravenously injected with 4×10^6 mixed bone marrow (BM) cells at a 1:1 ratio, isolated from age- and sex-matched CD45.2$^+$ B-WT or B-Asns and CD45.1$^+$ WT donor mice. Recipient mice were maintained on antibiotics (Baytril, Bayer corporation) administered in their drinking water for two weeks. Bone marrow reconstitution was

confirmed by flow cytometry of peripheral blood at 8 weeks. Mice were immunised with SRBC at 11 weeks post-procedure and analysed at day 9.

Immunisation

For intraperitoneal SRBC immunisation, 1ml of sterile SRBCs (ThermoFisher) were washed twice with 15ml of ice-cold PBS and reconstituted in 3ml of PBS, and 200µl injected intraperitoneally. In some experiments, an enhanced SRBC immunisation method was used to maximise GC B cell yield by immunising mice with 0.1ml SRBC on day 0 followed by a second injection of 0.2ml on day 5 (Dominguez-Sola et al., 2015)[39]. For protein antigen immunisations, 50µg $NP_{(30-39)}$-CGG (Biosearch Tech) was mixed with Alum (ThermoFisher) at a 1:1 ratio and rotated at room temperature for 30 mins before intraperitoneal injection in 100µl PBS.

Asparaginase treatment

Blimp1-Venus mice were immunised with SRBC, and 50IU of asparaginase diluted in PBS from *E. coli* (Abcam) was administered by intraperitoneal injection at days 2 and 4.

Cell isolation

Spleens were dissociated by passing through 70µm cell strainers. For ex vivo GC B cell mass spectrometry, GC B cells were first enriched using the mouse Germinal Center B Cell (PNA) MicroBead Kit (Miltenyi), and then purified by flow sorting (Live/Dead$^-$CD19$^+$IgD$^-$GL-7$^+$CD95$^+$). Total B cells from the same mouse pool were pre-enriched using CD19$^+$ Microbeads (Miltenyi), then naïve B cells purified by flow sorting (Live/Dead$^-$B220$^+$IgD$^+$). To isolate cells for RNA extraction, GC B cells (Live/Dead$^-$CD19$^+$IgD$^-$CD95$^+$GL-7$^+$) and naïve B cells (Live/Dead$^-$CD19$^+$IgD$^+$) were flow sorted into RLT Plus buffer (Qiagen) following pre-enrichment with the Pan B Cell Isolation Kit II (Miltenyi). B cells for culture were isolated using the Pan B Cell Isolation Kit II (Miltenyi). Purity was routinely >90% by flow cytometry.

For some experiments, untouched GC B cells were isolated using a magnetic bead-based protocol as described[40]. Briefly, spleens were harvested from SRBC-immunised mice (enhanced protocol) and single cell suspensions were prepared in ice cold MACS isolation buffer (PBS with 0.5% BSA and 2mM EDTA) followed by ACK (Gibco) RBC lysis for 4 mins at 20°C with occasional mixing every 30s. After washing, cells were labelled with anti-CD43 microbeads (Miltenyi) and biotinylated antibodies against CD38 and CD11c (both eBioscience, clones 90 and N418 respectively), followed by incubation with anti-biotin microbeads (Miltenyi), and subsequently run through a MACS LS column (Miltenyi). Purity was confirmed by flow cytometry and immunocytochemistry and exceeded 95%.

Cell culture

Total B cells were isolated as described above. B cells were cultured at 3×10^6 cells/ml in RPMI1640 (custom product from Cell Culture Technologies, Gravesano, Switzerland, lacking glutamate, aspartate, glutamine, and asparagine), supplemented with 1mM pyruvate, 10mM HEPES, 100 IU/ml penicillin/streptomycin and 50µM 2-mercaptoethanol, and 10% dialysed FBS, containing the indicated concentration of Asn, Asp (150µM), Glu (140µM), GlutaMAX (Thermo or Sigma)(2mM), except where mentioned otherwise. B cells were stimulated with agonistic anti-CD40 (5µg/ml, FGK45.4, functional grade, Miltenyi), recombinant IL-4 (1ng/ml, Peprotech), or CpG (100nM, ODN1826, Miltenyi). For proliferation experiments, cells were

labelled with CellTrace Violet according to manufacturer's instructions (Thermo) before stimulation. For stable isotope labelling, ^{15}N(amide)-asparagine (485896, Merck) (400µM), ^{15}N(amide)-glutamine (NLM-557, Cambridge Isotope Laboratories) (2mM), ^{15}N(amino)-glutamine (NLM-1016, Cambridge Isotope Laboratories) (2mM), or $^{13}C_5$-glutamine (CLM-1822, Cambridge Isotope Laboratories) (2mM) were used, replacing their unlabelled molecule in RPMI1640.

Flow cytometry

Spleens were dissociated by passing through 70µm cell strainers, and red cells lysed with ACK Lysis Buffer (Gibco). For Peyer's patch dissociation, a 40µm strainer (VWR) was used. Single cell suspensions were incubated with Fixable Viability Dye eFluor™ 780 (eBioscience) in PBS, followed by Fc Block (5 mins) and surface antibodies (30 mins on ice) in FACS buffer (PBS supplemented with 0.5% BSA and 2mM EDTA). For intracellular staining, cells were fixed in 4% paraformaldehyde at 20°C, then permeabilised with ice cold 90% methanol for 10 mins. To measure OPP ex vivo incorporation, cells were incubated in RPMI1640 with the indicated concentration of Asn, in the presence of 20µM OPP for 25 mins at 37°C. Click labelling was then performed with the Click-iT™ Plus OPP Alexa Fluor 647 Protein Synthesis Assay Kit (ThermoFisher, cat: C10458). 5-EU incorporation was measured by incubating cells with 5-EU (1mM) for 25 mins in RPMI1640 at 37°C, and then using the Click-iT™ RNA Alexa Fluor™ 594 Imaging Kit (ThermoFisher, cat: C10330) according to manufacturer's instructions. Mitochondrial dye staining was performed with MitoTracker Green (100nM, Thermo) or MitoSOX (10µM, Thermofisher) for 30 mins in RPMI1640 at 37°C. NP binding was determined by incubation with NP-PE (Biosearch) for 30 mins at 4°C. Apoptosis was quantified by annexin V-FITC binding (Biolegend). The proliferation index was determined using the Proliferation module of FlowJo (BD).

Antibody (Catalogue number)	**Clone**	**Manufacturer**
Anti-GL-7 (144612)	GL-7	Biolegend
Anti-CD138(142504)	281-2	Biolegend
Anti-CD19 (115538)	6D5	Biolegend
Anti-IgD (405721)	11-26c-2a	Biolegend
Anti-CD38 (102718)	90	Biolegend
Anti-CXCR4 (146513)	L276F12	Biolegend
Anti-CD98 (128211)	RL388	Biolegend
Anti-IgG1 (406617)	RMG1-1	Biolegend
Anti-MHCII (107605)	M5/114.15.2	Biolegend
Anti-Igλ(407306)	RML-42	Biolegend
Anti-CD23 (101608)	B3B4	Biolegend
Anti-CD43 (12-0431-82)	eBioR2/60	ThermoFisher
CD86 (105031)	GL-1	Biolegend
B220 (103247)	RA3-6B2	Biolegend
IgM (406513)	RMM-1	Biolegend
CD21 (123409)	7E9	Biolegend
Anti-TACI (133403)	8F10	Biolegend
Fixable viability dye 780		ThermoFisher
Anti-CD16/32 (Fc Block)	2.4G2	ThermoFisher

Immunofluorescence microscopy

Splenic sections were fixed overnight in Antigenfix (DiaPath) solution at 4°C. The next day, spleens were washed in PBS, followed by overnight incubation in 30% sucrose (in PBS) at 4°C for cryoprotection. On the following day, spleens were snap frozen in 100% methanol on dry ice and stored at -80°C until cryosectioning at 8-12µm thickness. Slides were then rehydrated in PBS at 20°C, then permeabilised and blocked in PBS containing 0.1% Tween-20, 10% goat serum, and 10% rat serum at RT for two hours. All primary antibody staining was performed overnight at 4°C in PBS supplemented with 2% goat serum and 0.1% Tween-20. The following antibodies were used: anti-GL-7 (GL-7) and anti-IgD (11-26c.2a), both from Biolegend.

To visualise protein synthesis in vivo, mice were immunised with SRBC using the enhanced protocol. At day 14, they were injected intraperitoneally with 1.5mg L-AHA (Thermo) and then 4 hours later 1mg OPP (Jena Bioscience) dissolved in 100µl PBS, or PBS alone as a negative control. Mice were sacrificed 1h later, and spleens were harvested for immunofluorescence analysis. L-AHA and OPP were detected by Click Chemistry using the Click-iT™ Plus L-AHA and then Click-iT™ Plus OPP Alexa Fluor™ 488 or 647 Protein Synthesis kits (Thermo) following the manufacturer's protocols.

Slides were mounted with Fluoromount G (Southern Biotech, cat: 0100-01) and imaged using a Zeiss LSM 980 equipped with an Airyscan 2 module.

Mass spectrometry

To extract molecules, cell were pelleted and washed twice with cold PBS and once with ice cold ammonium acetate (150mM, pH 7.3). The pellet was then resuspended in 1ml 80% LC/MS grade methanol/ ultrapure water chilled on dry ice. The samples were vortexed three times on dry ice, and then centrifuged at 15,000×g for 5 mins. The initial supernatant was then transferred into a 1.8ml glass vial, and the pellet resuspended in 200µl 80% methanol as above, then centrifuged again at 15,000×g for 5 mins. The second supernatant was then combined with the first, dried at 4°C using a Centrivap (Conco), then stored at -80°C until analysis.

Dried metabolites were resuspended in 50% ACN:water and 1/10th was loaded onto a Luna 3µm NH_2 100A (150 × 2.0 mm) column (Phenomenex). The chromatographic separation was performed on a Vanquish Flex (Thermo Scientific) with mobile phases A (5mM NH_4AcO pH 9.9) and B (ACN) and a flow rate of 200µl/min. A linear gradient from 15% A to 95% A over 18 min was followed by 7 min isocratic flow at 95% A and reequilibration to 15% A. Metabolites were detected with a Thermo Scientific Q Exactive mass spectrometer run with polarity switching (+3.5 kV/– 3.5 kV) in full scan mode with an m/z range of 70-975 and 140.000 resolution. Maven (v8.1.27.11) was used to quantify the targeted metabolites by area under the curve using expected retention time (as determined with pure standards) and accurate mass measurements (< 5 ppm). Values were normalized to cell number. Relative amounts of metabolites were calculated by summing up the values for all measured isotopologues of the targeted metabolites. Metabolite Isotopologue Distributions were corrected for natural ^{15}N abundance. Metabolite and transcriptome data were analysed using MetaboAnalyst[41] and statistical analysis was performed in R.

Western blotting

Cells were lysed on ice in RIPA buffer (Merck) supplemented with protease and phosphatase inhibitors (cOmplete™ ULTRA Tablets and PhosSTOP™, Roche) for 30mins with frequent vortexing, and then centrifuged at 15,000×g for 15mins at 4°C and the supernatant recovered. Protein was quantified using the BCA method (Pierce, Thermo). Samples were denatured in Laemmli buffer (BioRad) containing 10% β-mercaptoethanol at 90°C for 5 mins then transferred to ice, before running on a 4-15% gel (Mini-PROTEAN TGX Precast Gels, BioRad). Protein was transferred onto PVDF membranes (BioRad), which were blocked in 2.5% skimmed milk for 1h, and then stained with the primary antibody diluted in 2.5% milk/0.05% TBS-Tween20 at 4°C overnight. The following primary antibodies were used: anti-ASNS (Proteintech), anti-ATF4 (D4B8), anti-p4E-BP1 (Thr37/46) (236B4), anti-vinculin (E1E9V), all from Cell Signalling Technologies.

Following washing, membranes were then incubated with horseradish peroxidase (HRP)-conjugated goat anti-rabbit secondary antibody in 2.5% milk/0.05% TBS-Tween20 for 1h at RT. Chemiluminescence was used to detect the secondary antibody (Anti-rabbit IgG, HRP-linked Antibody #7074 and SuperSignal™ West Pico PLUS Chemiluminescent Substrate, Thermo).

Quantitative PCR

Cells were washed in PBS and lysed in RLT Plus buffer (Qiagen) supplemented with 1% β-mercaptoethanol. RNA extraction was performed according to manufacturer's instructions using an RNeasy Plus Mini Kit (Qiagen). Reverse transcription was performed using the High Capacity RNA-to-cDNA Kit (Thermo). Quantitative qPCR was performed using Taqman Probes (Thermo). Relative expression was calculated with reference to *Ubc* or *Hprt*.

List of probes used:

Gene	Taqman ProbeID
Asns	Mm00803785_m1
Ubc	Mm02525934_g1
Hprt	Mm03024075_m1
Atf4	Mm00515325_g1
Dhodh	Mm00498393_m1
Adsl	Mm00507759_m1
Umps	Mm00801991_m1
Cad	Mm01216345_m1
Ppat	Mm00549096_m1
Atic	Mm00546563_m1
Pfas	Mm01325237_m1
Got2	Mm00494703_m1
Zbtb1	Mm01281881_m1

RNA sequencing

RNA was quantified using RiboGreen (Invitrogen) on the FLUOstar OPTIMA plate reader (BMG Labtech) and the size profile and integrity analysed on the 2200 or 4200 TapeStation (Agilent, RNA ScreenTape). RIN estimates were between 9.3 and 9.7. Input material was normalised to 100 ng prior to library preparation. Polyadenylated transcript enrichment and

strand specific library preparation was completed using NEBNext Ultra II mRNA kit (NEB) following manufacturer's instructions. Libraries were amplified (17 cycles) on a Tetrad (Bio-Rad) using in-house unique dual indexing primers (based on DOI: 10.1186/1472-6750-13-104). Individual libraries were normalised using Qubit, and the size profile was analysed on the 2200 or 4200 TapeStation. Individual libraries were normalised and pooled together accordingly. The pooled library was diluted to ~10 nM for storage. The 10 nM library was denatured and further diluted prior to loading on the sequencer. Paired end sequencing was performed using a NovaSeq6000 platform (Illumina, NovaSeq 6000 S2/S4 reagent kit, 300 cycles).

Transcripts were counted using *Salmon*, and differential gene expression and pathway analysis performed using the R packages *DESeq2* and *fgsea*.

Statistical analysis

The use of the statistical tests is indicated in the respective figure legends, with the error bars indicating the mean ± S.E.M. P values ≤ 0.05 were considered to indicate significance. Analyses were performed with GraphPad Prism v9 or R 4.1. No statistical methods were used to pre-determine sample sizes, but our sample sizes are similar to those reported in previous publications. The distribution of data was determined using normality testing to determine appropriate statistical methodology, or otherwise assumed to be normally distributed. For in vivo experiments we matched the age of the mice in experimental batches, but other modes of randomization were not performed. Data collection and analysis were not performed blind to the conditions of the experiments in most of the experiments.

Data availability

RNA sequencing data has been uploaded to GEO under accession number GSE228845

Code availability

This paper does not report novel code.

Author contributions

E.M. and A.C. conceived and designed the study. E.M., K.B., and Y.Y. performed experiments. A.C. and E.M. analysed metabolomic and transcriptional data. A.C. wrote the manuscript and supervised the study.

Acknowledgements

We thank Johanna ten Hoeve-Scott (UCLA Metabolomics Center, United States) for performing metabolomics studies. We thank Sarah Lamble (Oxford Genomics Centre) for performing RNA sequencing studies. We also thank Jonathan Webber for flow sorting and the BSU staff for support (Kennedy Institute of Rheumatology, University of Oxford). Funding for this work was provided by the Wellcome Trust (211072/Z/18/Z) and Cancer Research UK/Versus Arthritis (C70663/A29547) to A.C. For the purpose of open access, the author has applied a CC BY-ND public copyright license to any Author Accepted Manuscript version arising from this submission. The computational aspects of this research were supported by the Wellcome Trust Core Award Grant Number 203141/Z/16/Z and the NIHR Oxford BRC. The views expressed are those of the author(s) and not necessarily those of the NHS, the NIHR or the Department of Health.

References

1. Victora, G. D. & Nussenzweig, M. C. Germinal Centers. *Annu. Rev. Immunol.* **40**, 413–442 (2022).
2. Boothby, M. & Rickert, R. C. Metabolic Regulation of the Immune Humoral Response. *Immunity* **46**, 743–755 (2017).
3. Chen, D. *et al.* Coupled analysis of transcriptome and BCR mutations reveals role of OXPHOS in affinity maturation. *Nat. Immunol.* 1–10 (2021) doi:10.1038/s41590-021-00936-y.
4. Weisel, F. J. *et al.* Germinal center B cells selectively oxidize fatty acids for energy while conducting minimal glycolysis. *Nat. Immunol.* **21**, 331–342 (2020).
5. Urbanczyk, S. *et al.* Mitochondrial respiration in B lymphocytes is essential for humoral immunity by controlling the flux of the TCA cycle. *Cell Rep.* **39**, 110912 (2022).
6. Luo, W. *et al.* SREBP signaling is essential for effective B cell responses. *Nat. Immunol.* 1–12 (2022) doi:10.1038/s41590-022-01376-y.
7. Cho, S. H. *et al.* Germinal centre hypoxia and regulation of antibody qualities by a hypoxia response system. *Nature* **537**, 234–238 (2016).
8. Geiger, R. *et al.* L-Arginine Modulates T Cell Metabolism and Enhances Survival and Anti-tumor Activity. *Cell* **167**, 829-842.e13 (2016).
9. Ron-Harel, N. *et al.* Mitochondrial Biogenesis and Proteome Remodeling Promote One-Carbon Metabolism for T Cell Activation. *Cell Metab.* **24**, 104–117 (2016).
10. Sinclair, L. V. *et al.* Control of amino-acid transport by antigen receptors coordinates the metabolic reprogramming essential for T cell differentiation. *Nat. Immunol.* **14**, 500–508 (2013).
11. Fernández-García, J. *et al.* CD8+ T cell metabolic rewiring defined by scRNA-seq identifies a critical role of ASNS expression dynamics in T cell differentiation. *Cell Rep.* **41**, (2022).
12. Wu, J. *et al.* Asparagine enhances LCK signalling to potentiate CD8 + T-cell activation and anti-tumour responses. *Nat. Cell Biol.* **23**, 75–86 (2021).
13. Kelly, B. & Pearce, E. L. Amino Assets: How Amino Acids Support Immunity. *Cell Metab.* S1550413120303119 (2020) doi:10.1016/j.cmet.2020.06.010.
14. Eraslan, Z., Papatzikas, G., Cazier, J.-B., Khanim, F. L. & Günther, U. L. Targeting Asparagine and Serine Metabolism in Germinal Centre-Derived B Cells Non-Hodgkin Lymphomas (B-NHL). *Cells* **10**, 2589 (2021).
15. Parsa, S. *et al.* The serine hydroxymethyltransferase-2 (SHMT2) initiates lymphoma development through epigenetic tumor suppressor silencing. *Nat. Cancer* **1**, 653–664 (2020).
16. D'Avola, A. *et al.* PHGDH is required for germinal center formation and is a therapeutic target in MYC-driven lymphoma. *J. Clin. Invest.* **132**, e153436 (2022).
17. Grima-Reyes, M. *et al.* Tumoral microenvironment prevents de novo asparagine biosynthesis in B cell lymphoma, regardless of ASNS expression. *Sci. Adv.* **8**, eabn6491 (2022).
18. Cantor, J. *et al.* CD98hc facilitates B cell proliferation and adaptive humoral immunity. *Nat. Immunol.* **10**, 412–419 (2009).
19. Dieterich, D. C., Link, A. J., Graumann, J., Tirrell, D. A. & Schuman, E. M. Selective identification of newly synthesized proteins in mammalian cells using bioorthogonal noncanonical amino acid tagging (BONCAT). *Proc. Natl. Acad. Sci.* **103**, 9482–9487 (2006).
20. Painter, M. W. *et al.* Transcriptomes of the B and T Lineages Compared by Multiplatform Microarray Profiling. *J. Immunol.* **186**, 3047–3057 (2011).
21. Müller-Winkler, J. *et al.* Critical requirement for BCR, BAFF, and BAFFR in memory B cell survival. *J. Exp. Med.* **218**, e20191393 (2020).

22. Lomelino, C. L., Andring, J. T., McKenna, R. & Kilberg, M. S. Asparagine synthetase: Function, structure, and role in disease. *J. Biol. Chem.* **292**, 19952–19958 (2017).
23. Hobeika, E. *et al.* Testing gene function early in the B cell lineage in mb1-cre mice. *Proc. Natl. Acad. Sci. U. S. A.* **103**, 13789–13794 (2006).
24. Smith, F. I., Tesch, H. & Rajewsky, K. Heterogeneous and monoclonal helper T cells induce similar anti-(4-hydroxy-3-nitrophenyl)acetyl (NP) antibody populations in the primary adoptive response II. Lambda light chain dominance and idiotope expression. *Eur. J. Immunol.* **14**, 195–200 (1984).
25. Akiyama, T., Kobayashi, K., Higashikage, A., Sato, J. & Yoshinaga, H. CSF/plasma ratios of amino acids: Reference data and transports in children. *Brain Dev.* **36**, 3–9 (2014).
26. Sullivan, L. B. *et al.* Aspartate is an endogenous metabolic limitation for tumour growth. *Nat. Cell Biol.* 1–12 (2018) doi:10.1038/s41556-018-0125-0.
27. Crawford, J. & Cohen, H. J. The essential role of L-glutamine in lymphocyte differentiation in vitro. *J. Cell. Physiol.* **124**, 275–282 (1985).
28. Harding, H. P. *et al.* An Integrated Stress Response Regulates Amino Acid Metabolism and Resistance to Oxidative Stress. *Mol. Cell* **11**, 619–633 (2003).
29. Pakos-Zebrucka, K. *et al.* The integrated stress response. *EMBO Rep.* **17**, 1374–1395 (2016).
30. Williams, R. T. *et al.* ZBTB1 Regulates Asparagine Synthesis and Leukemia Cell Response to L-Asparaginase. *Cell Metab.* **31**, 852-861.e6 (2020).
31. Krall, A. S., Xu, S., Graeber, T. G., Braas, D. & Christofk, H. R. Asparagine promotes cancer cell proliferation through use as an amino acid exchange factor. *Nat. Commun.* **7**, 1–13 (2016).
32. Krall, A. S. *et al.* Asparagine couples mitochondrial respiration to ATF4 activity and tumor growth. *Cell Metab.* S1550413121000577 (2021) doi:10.1016/j.cmet.2021.02.001.
33. Hope, H. C. *et al.* Coordination of asparagine uptake and asparagine synthetase expression modulates CD8$^+$ T cell activation. *JCI Insight* **6**, (2021).
34. Pengo, N. *et al.* Plasma cells require autophagy for sustainable immunoglobulin production. *Nat. Immunol.* **14**, 298–305 (2013).
35. Di Conza, G., Ho, P.-C., Cubillos-Ruiz, J. R. & Huang, S. C.-C. Control of immune cell function by the unfolded protein response. *Nat. Rev. Immunol.* 1–17 (2023) doi:10.1038/s41577-023-00838-0.
36. Rossi, M. *et al.* PHGDH heterogeneity potentiates cancer cell dissemination and metastasis. *Nature* **605**, 747–753 (2022).
37. Ben-Sahra, I., Howell, J. J., Asara, J. M. & Manning, B. D. Stimulation of de Novo Pyrimidine Synthesis by Growth Signaling Through mTOR and S6K1. *Science* **339**, 1323–1328 (2013).
38. Ben-Sahra, I., Hoxhaj, G., Ricoult, S. J. H., Asara, J. M. & Manning, B. D. mTORC1 induces purine synthesis through control of the mitochondrial tetrahydrofolate cycle. *Sci. N. Y. NY* **351**, 728–733 (2016).
39. Dominguez-Sola, D. *et al.* The FOXO1 Transcription Factor Instructs the Germinal Center Dark Zone Program. *Immunity* **43**, 1064–1074 (2015).
40. Cato, M. H., Yau, I. W. & Rickert, R. C. Magnetic-based purification of untouched mouse germinal center B cells for ex vivo manipulation and biochemical analysis. *Nat. Protoc.* **6**, 953–960 (2011).
41. Xia, J., Sinelnikov, I. V., Han, B. & Wishart, D. S. MetaboAnalyst 3.0—making metabolomics more meaningful. *Nucleic Acids Res.* **43**, W251–W257 (2015).